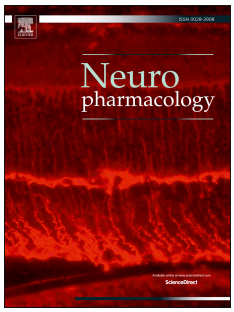

Activation of adenosine A_{2A} receptors in the olfactory tubercle promotes sleep in rodents

Rui Li, Yi-Qun Wang, Wen-Ying Liu, Meng-Qi Zhang, Lei Li, Yoan Cherasse, Serge N. Schiffmann, Alban de Kerchove d'Exaerde, Michael Lazarus, Wei-Min Qu, Zhi-Li Huang

PII: S0028-3908(19)30494-0

DOI: https://doi.org/10.1016/j.neuropharm.2019.107923

Reference: NP 107923

To appear in: *Neuropharmacology*

Received Date: 15 June 2019

Revised Date: 1 December 2019

Accepted Date: 20 December 2019

Please cite this article as: Li, R., Wang, Y.-Q., Liu, W.-Y., Zhang, M.-Q., Li, L., Cherasse, Y., Schiffmann, S.N., de Kerchove d'Exaerde, A., Lazarus, M., Qu, W.-M., Huang, Z.-L., Activation of adenosine A_{2A} receptors in the olfactory tubercle promotes sleep in rodents, *Neuropharmacology* (2020), doi: https://doi.org/10.1016/j.neuropharm.2019.107923.

Title: Activation of adenosine A_{2A} receptors in the olfactory tubercle promotes sleep in rodents

Rui Li[a,b,c,1], Yi-Qun Wang[a,b,c,1], Wen-Ying Liu[a,b,c,1], Meng-Qi Zhang[a,b,c], Lei Li[a,b,c], Yoan Cherasse[d], Serge N. Schiffmann[e], Alban de Kerchove d'Exaerde[e], Michael Lazarus[d], Wei-Min Qu[a,b,c], Zhi-Li Huang[a,b,c,*]

[a] Department of Pharmacology and Shanghai Key Laboratory of Bioactive Small Molecules, School of Basic Medical Science; State Key Laboratory of Medical Neurobiology, Institutes of Brain Science and Collaborative Innovation Centre for Brain Science, Fudan University, Shanghai, 200032, China

[b] Institute for Basic Research on Aging and Medicine, School of Basic Medical Sciences, Fudan University, Shanghai, 200032, China

[c] Shanghai Key Laboratory of Clinical Geriatric Medicine, Fudan University, Shanghai, 200032, China

[d] International Institute for Integrative Sleep Medicine (WPI-IIIS), University of Tsukuba, Tsukuba, 305-8577, Japan

[e] Laboratory of Neurophysiology, ULB Neuroscience Institute, Université Libre de Bruxelles, 1050 Brussels, Belgium

[1] R.L., Y.Q.W., and W.Y.L contributed equally.

* Corresponding author. E-mail address: huangzl@fudan.edu.cn

Abstract

The olfactory tubercle (OT), an important nucleus in processing sensory information, has been reported to change cortical activity under odor. However, little is known about the physiological role and mechanism of the OT in sleep-wake regulation. The OT expresses abundant adenosine A_{2A} receptors (A_{2A}Rs), which are important in sleep regulation. Therefore, we hypothesized that the OT regulates sleep via A_{2A}Rs. This study examined sleep-wake profiles through electroencephalography and electromyography recordings with pharmacological and chemogenetic manipulations in freely moving rodents. Compared with their controls, activation of OT A_{2A}Rs pharmacologically and OT A_{2A}R neurons via chemogenetics increased non-rapid eye movement sleep for 3 and 5 hours, respectively, while blockade of A_{2A}Rs decreased non-rapid eye movement sleep. Tracing and electrophysiological studies showed OT A_{2A}R neurons projected to the ventral pallidum and lateral hypothalamus, forming inhibitory innervations. Together, these findings indicate that A_{2A}Rs in the OT play an important role in sleep regulation.

Keywords: Olfactory tubercle; Adenosine A_{2A} receptors; Non-rapid eye movement sleep; Chemogenetics

Abbreviation: A_{2A}R, adenosine A_{2A} receptor; aCSF, artificial cerebral spinal fluid; AP, anteroposterior; CNO, clozapine-N-oxide; DREADDs, designer receptors exclusively activated by designer drugs; DV, dorsoventral; hrGFP, humanized Renilla green fluorescent protein; LH, lateral hypothalamus; ML, mediolateral; NAc, nucleus

accumbens; NREM, non-rapid eye movement; OB, olfactory bulb; OT, olfactory tubercle; REM, rapid eye movement; RT-PCR, reverse transcription-polymerase chain reaction; vGAT, vesicular GABA transporter; vGluT2, vesicular glutamate transporter 2; VP, ventral pallidum.

1. Introduction

The olfactory tubercle (OT), one of the main components in the olfactory system, is located at the ventral surface of the brain in rodents, surrounded by the nucleus accumbens (NAc), the basal forebrain, and the limbic system (Xiong and Wesson, 2016). It is responsible for receiving and transmitting odor information from the olfactory bulb (OB) to other brain regions (Wesson and Wilson, 2011). The OT is involved in the ventral striatum reward circuit, and has been considered an integrative interface between odor and odor-induced behaviors (Wesson and Wilson, 2011). Rats with the unilateral lesioned OT are more likely to stay in a sleep state that is easier for food odor to evoke arousal (Gervais, 1979), suggesting that the OT is capable of affecting vigilance states. However, the physiological role and the fundamental mechanism of the OT in sleep-wake regulation remain unclear.

Adenosine is one of the most important endogenous sleep promoters in the brain (Huang et al., 2014; Lazarus et al., 2013), inducing sleep via its A_1 and A_{2A} receptors (A_{2A}Rs), with A_{2A}Rs being more important (Huang et al., 2011). Studies using immunohistochemistry and *in situ* hybridization have demonstrated that A_{2A}Rs are abundant in the OT (DeMet and Chicz-DeMet, 2002). The expression of A_{2A}Rs in the OT is decreased under acute sleep deprivation (Basheer et al., 2001) and chronic sleep restriction (Kim et al., 2015). Chronic infusion of CGS21680, a selective A_{2A}R agonist, into the rostral part of the basal forebrain promotes sleep (Hong et al., 2005) and increases expression of Fos in the medial part of the OT (Satoh et al., 1999). We

therefore hypothesized that the OT may regulate sleep via its A_{2A}Rs.

In this study, pharmacological manipulations of A_{2A}Rs in the OT by local injection of a selective agonist or antagonist were utilized to examine the role of OT A_{2A}Rs. Next, we investigated the function of OT A_{2A}R neurons on sleep regulation via chemogenetics, also known as designer receptors exclusively activated by designer drugs (DREADDs). The terminal fields of OT A_{2A}R neurons were examined by an adeno-associated virus (AAV), which expressed the humanized Renilla green fluorescent protein (hrGFP) under the control of the A_{2A}R promoter. In addition, an *in vitro* optogenetic approach was used to determine the neuronal circuit responsible for the function of OT A_{2A}R neurons. Our results clearly indicate that the activation of A_{2A}Rs and A_{2A}R neurons in the OT promotes non-rapid eye movement (NREM) sleep.

2. Methods and Materials

2.1 Animals and reagents

Male A_{2A}R-Cre mice on a background of C57BL/6 were well-validated in previous studies (Yuan et al., 2017; Zhang et al., 2013). The male Sprague-Dawley rats, which weighed between 280 and 320 grams, were acquired from the Animal Center of the Chinese Academy of Sciences (Shanghai, China). Animals were kept in a specific-pathogen-free, temperature (22±0.5°C) and humidity (60±2%) controlled environment, which also had a 12-12-hour light-dark cycle with lights on at 07:00 and illuminated at an intensity of 100 lux. Food and water were freely accessible to animals.

All experimental procedures were designed to lessen the required animal numbers, to reduce pain and discomfort, and were subjected to the approval of the Medical Experiment Animals Administrative Committee of Shanghai before experiments were carried out.

The selective $A_{2A}R$ agonist CGS21680 (Sigma, Saint Louis, MO, USA) was dissolved and then diluted 100 times in saline to achieve the desired concentration of 2 nmol/μl. Similarly, the selective $A_{2A}R$ antagonist KW6002 (Kaster et al., 2015) was suspended and diluted in 5% dimethyl sulphoxide saline to 52 nmol/μl. The volume of CGS21680 and KW6002 solutions was fixed at 0.3 μl. For *in vivo* experiments, Clozapine-N-oxide (CNO; Sigma) was dissolved in saline to a concentration of 0.3 mg/ml, and the volume of the CNO solution was calculated by body weight at 10 ml/kg. For in vitro experiments, the CNO was dissolved in aCSF and then diluted to 5 μM. The SR-95531 (Abcam Biochemicals, UK), NBQX (Tocris Bioscience, UK), or D-APV (Tocris Bioscience) was dissolved and diluted using aCSF to 5 μM. All solutions were freshly made right before use.

2.2 Surgical and Recording Procedures for Pharmacological Modulation of $A_{2A}Rs$ in the OT

After intraperitoneal (i.p.) pentobarbital (50 mg/kg) anesthesia, male rats were implanted with electroencephalogram (EEG) and electromyogram (EMG) recording headmounts and two guide cannulae (outer diameter =0.55 mm) for drug injection

according to our previous study (Wang et al., 2017). The two guide cannulae were inserted stereotaxically using the following coordinates (relative to bregma): anteroposterior (AP) +1.8 mm, mediolateral (ML) ±2.5 mm and dorsoventral (DV) +9.2 mm with a 30° angle against the vertical into the contralateral side. These rats were given a 10-day recovery period followed by a three-day habituation period before starting the recording session.

Based on manipulations, a 24-hour baseline starting at 19:00 for activation or 07:00 for blockade was obtained. Since the presumable effect of activation A_{2A}Rs in the OT was to increase NREM sleep and rats spend the least time in NREM sleep during the first half of the dark period, CGS21680 or the vehicle was injected at 21:00, while KW6002 or the vehicle were injected at 09:00. To ensure a minimal dorsal spread of the injected solution, cannulae were inserted at a 30-degree angle, and the solution (0.3 µl per side) was injected using a one-microliter Hamilton syringe bilaterally over one minute with an additional one-minute before withdrawing for each side. After recording, animals were sacrificed to verify the position of guide cannulae via Nissl's staining.

2.3 Surgical and Recording Procedures for Chemogenetic Activation of OT A_{2A}R Neurons in A_{2A}R-Cre mice

A_{2A}R-Cre mice, under pentobarbital anesthesia (50 mg/kg, i.p.), were infused with the AAV that contained Cre-dependent hM3Dq/hM4Di-mCherry (AAV-hSyn-DIO-hM3Dq/hM4Di-mCherry, 4×10^{12} particles/ml, 100 nl/side) into the OT so

that $A_{2A}R$ neurons can be specifically controlled (Oishi et al., 2017a; Wang et al., 2017). The coordinate of the OT was AP: +2.0 mm, ML: ±1.5 mm, and DV: -5.3 mm. EEG and EMG headmounts were then implanted according to previous studies (Qu et al., 2010; Zhang et al., 2017). These mice were given a three-week recovery period for transfection of the virus and then connected to the recording cable for a three-day habituation.

Polygraphic recording started at 19:00 and lasted for two days. OT-hM3Dq and OT-hM4Di mice received the vehicle and CNO (i.p.) at 21:00 and 09:00, respectively, on both days. After the previous CNO was totally washed out, OT-hM3Dq mice were injected with the vehicle or CNO. One and a half hours later, the animals were sacrificed to verify the virus microinjection site and c-Fos expression via immunohistochemistry.

2.4 Vigilance State Analysis

Raw EEG/EMG signals were amplified, filtered and digitized at a sampling rate of 128 Hz using *VitalRecorder* (Biotex, Kyoto, Japan). Vigilance states were determined off-line at 4-second epochs as wakefulness, NREM or REM sleep by *SleepSign* (Biotex, Kyoto, Japan) using a standard algorithm (Huang et al., 2005; Qu et al., 2010; Wang et al., 2015). The software-defined sleep-wake stages were visually examined, and necessary corrections were made.

2.5 Nissl's Staining

Rats with guide cannulae were perfused transcardially under pentobarbital

anesthesia (50 mg/kg, i.p.) with 0.1 M phosphate buffered saline (PBS), followed by 4% paraformaldehyde phosphate buffered solution. Brains were removed, post-fixed and dehydrated in graded phosphate-buffered sucrose solution up to 30%. The brains were then sliced into coronal sections on a cryostat into 30 μm slices. These brain slices were rinsed and mounted onto glass slides which were placed in a drying chamber to get rid of excessive moisture at room temperature for one week. Glass slides were then put into distilled water twice, cresyl violet acetate once, distilled water twice, 75% alcohol twice, 95% alcohol twice and xylene twice. After the last quench in xylene, the slides were wiped clean and sealed with resin.

2.6 Immunohistochemistry for DAB staining

Brains were processed as Nissl's staining. Immunohistochemistry was performed on free-floating sections as previously described (Lazarus et al., 2011; Wang et al., 2017). In brief, sections were briefly rinsed in PBS, incubated in 0.3% hydrogen peroxide in PBS (0.1 M) for 30 minutes at room temperature, and then incubated at room temperature in 3% normal donkey serum and 0.3% Triton X-100 in PBS for 1 h. The primary antibody was diluted in 0.3% Triton X-100 in PBS with 0.02% sodium azide and was left to react with brain slices at 4°C overnight. For double staining, the first primary antibody was rabbit anti-c-Fos (1:10000; Millipore). Sections were rinsed the next day and incubated for 2 h in biotinylated anti-rabbit secondary antiserum (1:1000; Jackson ImmunoResearch). Avidin-biotin-peroxidase complex (1:1000; Vector Laboratories) was applied to the brain

slices for 1 h and immunoreactive cells were visualized by reaction with 0.04% diaminobenzidine tetrahydrochloride (Sigma) and 0.01% hydrogen peroxide enhanced by nickel. The procedure above was conducted on the same section to examine the expression of hM3Dq by staining mCherry using the rat anti-mCherry (1:10000; Clontech) as the primary antibody and the anti-rat secondary antiserum without the additional nickel in the visualization. Finally, tissue sections were mounted on glass slides and observed under a light microscope.

In addition, a heat map was generated using fluorescence generated by hM3Dq-mCherry fusion protein to reveal the extension of hM3Dq expression according to a previous study (Wang et al., 2017) using MatLab R2015a (MathWorks).

2.7 Anterograde Tract-tracing

To understand the projection of OT $A_{2A}R$ neurons, $A_{2A}R$-Cre mice were bilaterally infused with AAV-lox-stop-hrGFP for anterograde tract-tracing according to coordinates used in the chemogenetic experiment. The hrGFP, which was encoded by the AAV vectors, was transcriptionally silenced by a Neo-cassette flanked by loxP sites. Therefore the expression of hrGFP was under the control of $A_{2A}R$ promoters (Gautron et al., 2010; Zhang et al., 2013). These $A_{2A}R$-Cre mice were sacrificed four weeks later and brain sections were obtained as aforementioned. After mounting the sections onto glass slides, the slides were sealed with Fluoromount-G (SouthernBiotech, Birmingham, AL, USA) to prevent the fluorescence quenching and were then observed and photographed

148 under a fluorescence microscope.

149

150 *2.8 Patch-clamp Electrophysiology for Verifying hM3Dq Functionality*

151 After a 4-week recovery, male A_{2A}R-Cre mice fully expressing
152 AAV-hSyn-DIO-hM3Dq-mCherry were studied. Heart perfusion was performed on these
153 mice under anesthesia (pentobarbital, 50 mg/kg, i.p.). Modified artificial cerebral spinal
154 fluid (aCSF), containing 213 mM sucrose, 10 mM glucose, 2.5 mM KCl, 1.25 mM
155 NaH_2PO_4, 26 mM $NaHCO_3$, 3 mM $MgSO_4$, 0.4 mM ascorbic acid and 0.1 mM $CaCl_2$
156 proceeded into the systemic circulation. To minimize the number of injured cells, the
157 mouse brain was quickly extracted from the skull after perfect perfusion while being
158 submerged in the perfusion solution at ~0°C. Coronal sections of the OT at a thickness
159 of 300 μm were prepared by a vibratome (VT-1200, Leica Microsystems, Germany).
160 Slices were then immediately placed in the holding chamber at ~32°C once they had
161 been cut and at least 30 minutes was needed for pre-recovery. Another 30 minutes was
162 set up for further recovery at ~0°C before being placed in the recording chamber at
163 ~32°C, which was superfused with bicarbonate-buffered solution containing 25 mM
164 glucose, 2 mM $CaCl_2$, 2.5 mM KCl, 1.25 mM NaH_2PO_4, 26 mM $NaHCO_3$, 1 mM $MgCl_2$
165 and 119 mM NaCl. All the solution above were saturated with 95% oxygen and 5%
166 carbon dioxide.

167 Putative A_{2A}R-expressing neurons in the OT were identified by the hM3Dq-mCherry
168 infusion protein using infrared differential interference contrast and fluorescence

169 microscopy. Recordings, including whole-cell current-clamp, were performed with the
170 help of an Axopatch 700B amplifier. Patch electrodes (4.0-7.0 MΩ) were backfilled with
171 internal solution containing 130 mM K-gluconate, 10 mM Hepes, 10 mM KCl, 0.5 mM
172 EGTA, 4 mM ATP-Mg, 0.5 mM GTP-Na, and 10 mM phosphocreatine (pH =7.5). Input
173 resistance was tested online through a 20-pA current injection (50 ms). The neurons
174 were first stably recorded in current-clamp mode for 2-5 min, and then 5 μM CNO was
175 perfused into the electrophysiological bath. All data acquired was filtered at 1 kHz and
176 digitized using p-Clamp 10.3 software (Molecular Devices, Sunnyvale, CA, USA).
177
178 *2.9 Optogenetic-assisted Patch-clamp Electrophysiology for Identifying Innervation*
179 *Properties of OT A_{2A}R Neurons*
180 Male A_{2A}R-Cre mice were anesthetized with pentobarbital (50 mg/kg, i.p.) four weeks
181 after being infused with AAV-hSyn-DIO-ChR2-mCherry. Brain slices containing the OT,
182 ventral pallidum (VP) and lateral hypothalamus (LH) were obtained as descried above.
183 We first examined the electrophysiological property of the recording neurons in the OT in
184 current-clamp by injection of step currents. The photostimulation (5-ms 473-nm light
185 pulses) to activate ChR2 was delivered at the OT via LED through the 40X objective lens.
186 Evoked postsynaptic currents from VP or LH neurons were triggered by photostimulation
187 (5-ms 473-nm light pulses) delivered at 10 Hz at the terminals of OT A_{2A}R neurons.
188 ACSF with the $GABA_A$ receptor antagonist SR-95531 (5 μM, abcam Biochemicals, UK)
189 or the AMPA/NMDA receptor antagonists NBQX (5 μM, Tocris Bioscience, UK) and

D-APV (25 μM, Tocris Bioscience, UK) were applied to the VP or LH slice to clarify the receptor type of the postsynaptic currents.

2.10 Single-cell Reverse Transcription-Polymerase Chain Reaction (RT-PCR)

The cytoplasms of OT $A_{2A}R$ neurons and responding neurons in the VP and LH were aspirated into the patch pipette after electrophysiological recording, and then dislodged into a PCR tube as previously described (Lambolez et al., 1992; Xu et al., 2015). The presence of mRNA coding either vesicular GABA transporter (vGAT) and vesicular glutamate transporter 2 (vGluT2) was tested separately using the following single-cell RT-PCR protocol. First, reverse transcription and the first round of PCR amplification were performed with gene-specific multiplex primers (the sequence for vGluT2 was as follows: Fwd: TGTTCTGGCTTCTGGTGTCTTACGAGAG; Rev: TTCCCGACAGCGTGCCAACA, and the sequence for vGAT was as follows: Fwd: ATTCAGGGCATGTTCGTGCT; Rev: ATGTGTGTCCAGTTCATCAT) using a 50 μl reaction system, which contained 25 μl 2× reaction mix, 20 μl H_2O, 1 μl of 10 μM sense primer, 1 μl of 10 μM anti-sense primer, 2 μl Platinum® Taq Mix, and 1 μl template RNA. Next, nested PCR was carried out for detecting vGluT2 mRNA with nested primer (the sequence was as follows: Fwd: AGGTACATAGAAGAGAGCATCGGGGAGA; Rev: CACTGTAGTTGTTGAAAGAATTTGCTTGCTC) using a 20 μl reaction system, which consisted of 2 μl of 10× Ex Taq Buffer (20 mM Mg^{2+} plus), 1.6 μl of 2.5 μM dNTP mixture, 0.4 μl of 10 μM sense primer, 0.4 μl of 10 μM anti-sense primer, 0.15 μl TaKaRa Ex Taq

(5 U/μl), 13.45 μl H_2O, and 2 μl template DNA. For detecting vGAT mRNA, semi-nested PCR was carried out using the same reaction system with semi-nested primer (Rev: TGATCTGGGCCACATTGACC). The amplified production was visualized via electrophoresis using a 2% agarose gel. The whole procedure and the handling of samples were done with extreme care to prevent RNA degradation and contamination.

2.11 Statistical Analysis

All results were represented as their means and standard error of the mean (means ± SEM). Statistical comparisons between two groups were made using either paired Student's *t*-test or one-way ANOVA. For changes in sleep-wake profiles, repeated ANOVA measures were carried out to analyze the difference between hourly amounts of each stage, followed by the post hoc Fisher's Probable Least-Squares Difference test. Only when *p*-values were less than 0.05 was the difference then considered significant.

3. Results

3.1 Pharmacological Activation of the A_{2A}Rs in the OT with CGS21680 increased NREM Sleep in Rats

We first examined the role of A_{2A}Rs in the OT on sleep regulation via site-specific pharmacological manipulation. The selective A_{2A}R agonist CGS21680 or the vehicle was bilaterally injected into the OT of rats. As shown in the typical examples (Fig. 1A and B), the CGS21680-injected rat showed a noticeable increase in NREM sleep compared to

the vehicle-injected rat. At 0.6 nmol/side, CGS21680 significantly increased hourly NREM sleep amount by 70, 46, 50, 81 and 114% during the consecutive five hours after the CGS21680 injection compared with the vehicle group, while the hourly amount of wakefulness after drug injection decreased by 25, 28, 30, 34 and 36% during the consecutive five hours (Fig. 1C). During 21:00-02:00, the total amount of NREM sleep increased by 68%, with a 31% decrease in wakefulness (Fig. 1D). The hourly amount and the total amounts of REM sleep, however, showed minimal changes. Compared with the vehicle group, the NREM sleep power density (Fig. 1E) after CGS21680 injection did not show a significant difference. After the EEG/EMG recording, animals were sacrificed and the implantation sites of the guide cannulae were confirmed by Nissl's staining (Fig. 1F). These results indicate that activation of OT A_{2A}Rs increases NREM sleep.

3.2 Pharmacological Blockade of A_{2A}Rs in the OT with KW6002 Decreased NREM Sleep in Rats

We then bilaterally injected the selective A_{2A}R antagonist KW6002 into the OT of freely behaving rats. As shown in the typical examples (Fig. 2A and B), the KW6002-treated rat demonstrated a decreased NREM sleep amount and a prolonged wakefulness compared with the vehicle-injected rat. The mean latency to NREM sleep after KW6002 injection increased from 16.2 minutes to 48.7 minutes (Fig. 2C). KW6002 at 15.6 nmol/side significantly decreased the amount of NREM sleep by 68% in the first hour after injection with wakefulness increasing by 53% (Fig. 2D). There are no

253 differences in REM sleep or subsequent sleep-wake profiles. These results suggest that
254 blockade of OT A_{2A}Rs decreases NREM sleep.
255
256 *3.3 Chemogenetic Activation of OT A_{2A}R Neurons Increased NREM Sleep in A_{2A}R-Cre*
257 *Mice*
258 The expression of A_{2A}Rs is not limited to neurons (Orr et al., 2015), and therefore,
259 we examined whether OT A_{2A}R neurons were involved in sleep regulation using the
260 DREADD technology. The DREADD method, when combined with a double-floxed
261 inverted (FLEX) orientation, enables remote and non-invasive control of specific neurons.
262 The excitatory hM3Dq (Gq-coupled) receptors are mutant muscarinic G-protein-coupled
263 receptors, which interact exclusively with the exogenous biologically inert compound
264 CNO (Armbruster et al., 2007). The AAV containing hM3Dq was infused bilaterally into
265 the OT of A_{2A}R-Cre mice. The expression of hM3Dq was controlled by both the human
266 synapsin promotor and A_{2A}R promotor, such that A_{2A}R neuron specificity was achieved
267 (Fig. 3A). After three weeks, whole-cell patch-clamp recordings in acute slices of the OT
268 (Fig. 3B) were obtained to test the response of a single hM3Dq-expressing OT A_{2A}R
269 neuron to CNO. Application of CNO (3 μM) to the OT A_{2A}R neurons increased the
270 membrane potential significantly (Fig. 3C). After EEG and EMG recordings, the animals
271 were sacrificed to determine to which extent the hM3Dq-mCherry fusion protein was
272 expressed in the OT. Brain sections of recorded mice were obtained and prepared, and a
273 heat map was generated according to the autofluorescence of mCherry protein (Fig. 3D).

We also determined the expression of the c-Fos after CNO injection (Fig. 3E-H). Immunostaining revealed that CNO greatly increased c-Fos immunoreactivity in the OT that was colocalized with mCherry expression in $A_{2A}R$ neurons.

The sleep-wake profiles were examined after CNO treatment. As shown in the typical examples (Fig. 3I and J), the CNO-treated mouse demonstrated increased NREM sleep when compared to the vehicle-treated mouse. CNO at 3.0 mg/kg significantly increased the hourly NREM sleep amount by 53, 35 and 45% during the first, second and third hours, respectively, while the hourly amount of wakefulness after CNO administration decreased by 21% during the second hour (Fig. 3K). The amount of NREM sleep during 21:00-24:00 increased by 44%, along with a 26% decrease in wakefulness (Fig. 3L). The amount of REM sleep during the same period showed no significant difference. Meanwhile, inhibition of OT $A_{2A}R$ neurons via hM4Di had no effect on sleep-wake profiles (Fig. 3M). These results indicate that the activation of OT $A_{2A}R$ neurons via hM3Dq increases NREM sleep.

3.4 Anterograde Tracing of OT $A_{2A}R$ Neurons in the OT in $A_{2A}R$-Cre Mice

To better understand the neuronal circuit responsible for the NREM promoting effect of OT $A_{2A}R$ neurons, we used a well-validated conditional anterograde tract tracing approach (Fig. 4A) (Yuan et al., 2017; Zhang et al., 2013). The injection site (Fig. 4B) was confirmed by the restricted expression of hrGFP at the OT. Terminals of OT $A_{2A}R$ neurons were found in the external plexiform layer of OB (Fig. 4C), secondary motor

295 cortex (Fig. 4D), ventral pallidum (VP) (Fig. 4E), piriform cortex (Pir), dorsal endopiriform
296 nucleus, ventral endopiriform nucleus (Fig. 4F), cortex-amygdala transition zone, dorsal
297 part of anterior amygdaloid area, anterior part of basomedial amygdaloid nucleus,
298 anterior cortical amygdaloid nucleus, nucleus of the lateral olfactory tract (Fig. 4G) and
299 lateral hypothalamus (LH) (Fig. 4H). These results suggest that the A_{2A}R-expressing
300 neurons in the OT are projecting neurons and are connected to the wake-promoting VP
301 and LH (Anaclet et al., 2015; Herrera et al., 2016; Venner et al., 2016).
302
303 *3.5 Photostimulation of OT A_{2A}R Neurons in the OT Evoked GABA Release in the VP*
304 *and LH in A_{2A}R-Cre Mice*
305 Given that OT A_{2A}R neurons projected to several brain regions that are associated
306 with sleep regulation, an optogenetic-assisted electrophysiology approach was utilized to
307 further clarify the properties of innervation between OT A_{2A}R neurons and neurons in the
308 VP or LH (Fig. 5A). Four weeks after injected with AAV-hSyn-DIO-ChR2-mCherry (Han
309 et al., 2014), the A_{2A}R-Cre mice were sacrificed, and the brain slices were prepared. The
310 OT A_{2A}R neurons were visualized by fluorescence of the mCherry fusion protein and the
311 electrophysiological property of the neuron was first studied (Fig. 5B). A 300-pA or a
312 -200-pA current was injected into the recording neuron and resulted in an increased firing
313 frequency or a decreased membrane potential, respectively. Two types of OT A_{2A}R
314 neurons have been recorded (Supplementary Fig. 1). Over 70% showed the MSN-like
315 properties (Warre et al., 2011). Photostimulation (5 Hz, 10 Hz and 20 Hz) elicited action

potentials (Fig. 5C) similar to those elicited by positive current injections. Single-cell RT-PCR using the aspirated cytoplasm of the recorded OT $A_{2A}R$ expressing neurons determined the existence of both vGAT and vGluT2 mRNAs (Fig. 5D, Supplementary Fig. 2A).

Next, we tested the innervation of the OT $A_{2A}R$ neurons to the VP and LH neurons. Compared with the aCSF condition, a 19% reduction and a 98% reduction in the mean values of photostimulation elicited spontaneous postsynaptic currents were observed in recorded VP neurons under the glutamate receptor blockade (D-APV (25 μM) and NBQX (5 μM)) and under glutamate and GABA receptor blockade (SR-95531 (5 μM)) conditions, respectively (Fig. 5E). Interestingly, a 97% reduction between glutamate receptor and glutamate and GABA receptor blockade condition showed statistical significance (Fig. 5E). However, when GABA receptor antagonist was applied first, the inward current was immediately abolished, and the decrease from further applying glutamate receptor antagonists showed no statistical significance (Fig. 5F). When photostimulation was delivered, 19 of 32 recorded neurons in the VP responded, demonstrating the innervation of the OT $A_{2A}R$ neurons (Fig. 5G). Single-cell RT-PCR showed both vGAT and vGluT2 mRNA in the innervated VP neurons (Fig. 5H, Supplementary Fig. 2B). These findings suggest VP neurons mainly received GABAergic inputs from the OT $A_{2A}R$ neurons.

Similarly, when compared with the aCSF condition, a 29% reduction and a 95% reduction in the mean values of photostimulation elicited spontaneous postsynaptic

currents were observed in recorded LH neurons under glutamate receptor blockade (D-APV (25 μM) and NBQX (5 μM)) and under both glutamate and GABA receptor blockade (SR-95531 (5 μM)) conditions, respectively (Fig. 5I). Interestingly, a 93% reduction between glutamate receptor and all receptor blockades was also shown statistical significance (Fig. 5I). However, when the GABA receptor antagonist was applied first, the spontaneous postsynaptic currents was immediately abolished, and the decrease from further applying glutamate receptor antagonists showed no statistical significance (Fig. 5J). When photostimulation was applied, eight of 33 neurons in the LH responded (Fig. 5K), with only the presence of vGAT mRNA detected (Fig. 5L, Supplementary Fig. 2C). These findings suggest although the terminals of OT $A_{2A}R$ neurons in the LH mainly release GABA, the innervated LH neurons are GABAergic.

Together, these results indicate that OT $A_{2A}R$ neurons form inhibitory innervations with neurons in the VP and LH.

4. Discussion

The OT has been reported to influence sleep-wake regulation via high-frequency electrical stimulation (Benedek et al., 1981). However, the neuronal mechanism is still unclear. In this study, we found that pharmacological and chemogenetic activation of OT $A_{2A}Rs$ and OT $A_{2A}R$ neurons, respectively, increases NREM sleep amounts with a decrease in wakefulness, whereas inhibition of OT $A_{2A}Rs$ and OT $A_{2A}R$ neurons has a minimum effect on suppressing NREM sleep. The excitatory and inhibitory manipulation

was delivered at different time of the day which resulted in several hours of increasing in NREM sleep and in an hour of reduced NREM sleep due to decreased sleep latency, respectively, suggesting that the excitability of these neurons may be modulated by adenosine, which requires further investigation using, for example, adenosine deaminase to control the adenosine concentration at different time of the day. Nonetheless, our results clearly suggest a NREM-promoting role of OT A_{2A}Rs and OT A_{2A}R neurons. The expression of A_{2A}Rs is mainly in the striatum, including the CPu and NAc (DeMet and Chicz-DeMet, 2002). Activation of CPu A_{2A}R neurons dramatically increases NREM sleep during active phase through inhibiting the external globus pallidus, whereas inhibition of these neurons decreases NREM sleep only during active phase (Yuan et al., 2017). Chemogenetic or optogenetic activation of NAc core A_{2A}R neurons robustly induces NREM sleep in A_{2A}R-Cre mice through inhibiting the VP (Oishi et al., 2017b). While the CPu is an integral part of motor control and is implicated in Parkinson's disease, the NAc is involved in motivational stimuli related sleep-wake alternation (Oishi et al., 2017b). Being a processing center for olfaction and a part of ventral striatum, the OT provides the anatomical foundation for odor and odor-evoked behaviors, for example, odor guided reward seeking and cortical arousal (Gervais, 1979; Murata et al., 2015). Chronic sleep deprivation decreases the density of A_{2A}Rs in the OT and CPu (Kim et al., 2015), suggesting differentiated roles of A_{2A}Rs in different brain region in reaction to the increasing sleep drive. Further investigation using genetically targeted lesion of OT A_{2A}R neurons will help to fully understand the role of OT A_{2A}R

neurons in sleep regulation. Combined, these data paint a picture of a unified NREM sleep promoting role of adenosine/A_{2A}R system with emphasis on different aspects of the behaviors.

Furthermore, by combining anterograde tracing and optogenetic-assisted electrophysiology, we revealed that OT A_{2A}R neurons form an inhibitory connection with the VP, presumably both GABAergic and glutamatergic VP neurons. Chemogenetic activation of GABAergic neurons in the basal forebrain region including the VP strongly promotes wakefulness and increases fast EEG power density, while activation of glutamatergic neurons in the same nuclei has little effect (Anaclet et al., 2015); this indicates that the OT promotes NREM sleep through GABAergic VP neurons. Our results also suggest that OT A_{2A}R neurons form an inhibitory innervation with GABAergic neurons in the LH. Activation of GABAergic neurons in the LH leads to wakefulness (Herrera et al., 2016; Venner et al., 2016) . Some of these neurons inhibit the ventrolateral preoptic nucleus (Venner et al., 2016), whereas others inhibit the thalamic reticular nucleus (Herrera et al., 2016). The OT A_{2A}R neurons may preferentially projects to one sub-group of GABAergic LH neurons, which results in fewer responding neurons between the OT and LH than those between the OT and VP. Unfortunately, *in vivo* optogenetic manipulation targeting the OT or its terminals in the VP and LH failed to change the sleep-wake profiles in this study. It is notable that terminals of OT A_{2A}R neurons in the LH and VP not only release GABA but also a small amount of glutamate. The role of this excitatory innervation remains unknown and may contribute to a negative

feedback circuit, which could cause *in vivo* optogenetic experiments to fail. Another possible explanation is that the OT contains dopamine D_1 receptor expressing neurons (Murata et al., 2015) and neurons in the OT are densely connected with each other (Xiong and Wesson, 2016), which could further complicate the outcome of *in vivo* studies. Nonetheless, OT $A_{2A}R$ neurons may promote NREM sleep by their projection to the VP and LH neurons.

The olfaction system has a profound relationship with sleep. For example, fragrant odorants are often used in traditional medicines for their hypnotic effect. Animal studies reveal that inhalation of valerian oil shortens the sleep onset and increases sleep duration (Komori et al., 2006), while other odorants may increase rapid eye movement (REM) sleep (Yamaoka et al., 2005). On the other side, predator odor leads to an initial increase in NREM sleep δ power and then to sleep disturbance such as increased wakefulness and increased sleep during active phase (Sharma et al., 2018). As two major components in the olfaction system, our studies suggest that the OB and OT affect sleep differently. We have previously shown that OB $A_{2A}R$ neurons suppress REM sleep (Wang et al., 2017), while OT $A_{2A}R$ neurons promotes NREM sleep. Anatomically, the OT receives monosynaptic glutamatergic input from the ventral part of the OB where tufted cells dominate (Imamura et al., 2011; Scott et al., 1980; Wesson and Wilson, 2011; Xiong and Wesson, 2016), whereas OB $A_{2A}R$ neurons, putatively mitral cells, innervate the Pir (Wesson and Wilson, 2011; Xiong and Wesson, 2016), of which the reaction to odor is mediated by sleep state (Barnes et al., 2011). These pieces of evidence strongly suggest

that there exist two different neuronal circuits in the olfaction system and possibly account for the contrast effects of different odorants on sleep regulation. Our data also showed a trend in increasing NREM sleep δ power after A_{2A}Rs in the OT being activated (Fig. 1E), supporting the notion that the OT conveys odor valence, linking odor information and behaviors (Gadziola et al., 2015). By deepening our understanding on mechanism and implication of odor and odor-related sleep changes, new therapies against sleep disorders such as insomnia could emerge.

Olfactory dysfunction is often associated with neurological diseases such as idiopathic REM sleep behavior disorder (Jennum et al., 2013), Alzheimer's disease (Murphy, 1999) and Parkinson's disease (Iranzo, 2013). Interestingly, sleep disorders and olfactory dysfunction appear prior to the major symptoms of these diseases, for example, tremor and rigidity in Parkinson's disease (Spiegelhalder et al., 2013). As a key structure in the olfaction system, the OT provides unique insight into how odors affect sleep regulation. Unilateral lesion of the OT leads to the likelihood of staying in a shallower sleep stage and predisposition to arousal by odor in animals (Gervais, 1979). It is possible that the OT may attenuate the incoming odor sense and help maintain sleep. Modulation of the OT activity through different odorants or specifically targeting A_{2A}R neurons during sleep may be a novel strategy to treat sleep disorders of neurological diseases. Our findings suggest that the adenosine/A_{2A}R system is not only involved in physiological but may also be an innate part of sense-related sleep regulation.

5. Conclusion

In conclusion, by utilizing a pharmacological approach and a genetically engineered system, including chemogenetics, neuron type specific anterograde tracing and optogenetic-assisted electrophysiology, we have demonstrated that the OT is an important sleep promoting area.

Funding and Disclosure

This study was supported in part by grants-in-aid for scientific research from the National Natural Science Foundation of China [grant number 81420108015, 31530035, 81701305 to Z.L.H.; grant number 81571295, 81871037 to Y.Q.W.; and grant number 31671099, 31871072 to W.M.Q.]; the National Basic Research Program of China [grant number 2015CB856401 to Z.L.H.]; Shanghai Municipal Science and Technology Major Project [grant number 2018SHZDZX01 to Z.L.H.] and ZJLab; and Program for Shanghai Outstanding Academic Leaders to Z.L.H..

Declaration of interest

The authors declare no competing interests.

Acknowledgements

We would like to thank Dr. Jiang-Fan Chen for him kindly providing the $A_{2A}R$ antagonist KW6002.

463

464

References

Anaclet, C., Pedersen, N. P., Ferrari, L. L., Venner, A., Bass, C. E., Arrigoni, E., Fuller, P. M., 2015. Basal forebrain control of wakefulness and cortical rhythms. Nat Commun 6, 8744.

Armbruster, B. N., Li, X., Pausch, M. H., Herlitze, S., Roth, B. L., 2007. Evolving the lock to fit the key to create a family of G protein-coupled receptors potently activated by an inert ligand. Proc Natl Acad Sci U S A 104, 5163-5168.

Barnes, D. C., Chapuis, J., Chaudhury, D., Wilson, D. A., 2011. Odor fear conditioning modifies piriform cortex local field potentials both during conditioning and during post-conditioning sleep. PLoS One 6, e18130.

Basheer, R., Halldner, L., Alanko, L., McCarley, R. W., Fredholm, B. B., Porkka-Heiskanen, T., 2001. Opposite changes in adenosine A1 and A2A receptor mRNA in the rat following sleep deprivation. Neuroreport 12, 1577-1580.

Benedek, G., Obal, F., Jr., Rubicsek, G., Obal, F., 1981. Sleep elicited by olfactory tubercle stimulation and the effect of atropine. Behav Brain Res 2, 23-32.

DeMet, E. M., Chicz-DeMet, A., 2002. Localization of adenosine A2A-receptors in rat brain with [3H]ZM-241385. Naunyn Schmiedebergs Arch Pharmacol 366, 478-481.

Gadziola, M. A., Tylicki, K. A., Christian, D. L., Wesson, D. W., 2015. The olfactory tubercle encodes odor valence in behaving mice. J Neurosci 35, 4515-4527.

Gautron, L., Lazarus, M., Scott, M. M., Saper, C. B., Elmquist, J. K., 2010. Identifying the efferent projections of leptin-responsive neurons in the dorsomedial hypothalamus

using a novel conditional tracing approach. J Comp Neurol 518, 2090-2108.

Gervais, R., 1979. Unilateral lesions of the olfactory tubercle modifying general arousal effects in the rat olfactory bulb. Electroencephalogr Clin Neurophysiol 46, 665-674.

Han, Y., Shi, Y. F., Xi, W., Zhou, R., Tan, Z. B., Wang, H., Li, X. M., Chen, Z., Feng, G., Luo, M., Huang, Z. L., Duan, S., Yu, Y. Q., 2014. Selective activation of cholinergic basal forebrain neurons induces immediate sleep-wake transitions. Curr Biol 24, 693-698.

Herrera, C. G., Cadavieco, M. C., Jego, S., Ponomarenko, A., Korotkova, T., Adamantidis, A., 2016. Hypothalamic feedforward inhibition of thalamocortical network controls arousal and consciousness. Nat Neurosci 19, 290-298.

Hong, Z. Y., Huang, Z. L., Qu, W. M., Eguchi, N., Urade, Y., Hayaishi, O., 2005. An adenosine A receptor agonist induces sleep by increasing GABA release in the tuberomammillary nucleus to inhibit histaminergic systems in rats. J Neurochem 92, 1542-1549.

Huang, Z. L., Qu, W. M., Eguchi, N., Chen, J. F., Schwarzschild, M. A., Fredholm, B. B., Urade, Y., Hayaishi, O., 2005. Adenosine A2A, but not A1, receptors mediate the arousal effect of caffeine. Nat Neurosci 8, 858-859.

Huang, Z. L., Urade, Y., Hayaishi, O., 2011. The role of adenosine in the regulation of sleep. Curr Top Med Chem 11, 1047-1057.

Huang, Z. L., Zhang, Z., Qu, W. M., 2014. Roles of adenosine and its receptors in sleep-wake regulation. Int Rev Neurobiol 119, 349-371.

507 Imamura, F., Ayoub, A. E., Rakic, P., Greer, C. A., 2011. Timing of neurogenesis is a
508 determinant of olfactory circuitry. Nat Neurosci 14, 331-337.
509 Iranzo, A., 2013. Parkinson disease and sleep: sleep-wake changes in the premotor
510 stage of Parkinson disease; impaired olfaction and other prodromal features. Curr
511 Neurol Neurosci Rep 13, 373.
512 Jennum, P., Mayer, G., Ju, Y. E., Postuma, R., 2013. Morbidities in rapid eye movement
513 sleep behavior disorder. Sleep Med 14, 782-787.
514 Kaster, M. P., Machado, N. J., Silva, H. B., Nunes, A., Ardais, A. P., Santana, M., Baqi, Y.,
515 Muller, C. E., Rodrigues, A. L., Porciuncula, L. O., Chen, J. F., Tome, A. R., Agostinho,
516 P., Canas, P. M., Cunha, R. A., 2015. Caffeine acts through neuronal adenosine A2A
517 receptors to prevent mood and memory dysfunction triggered by chronic stress. Proc
518 Natl Acad Sci U S A 112, 7833-7838.
519 Kim, Y., Elmenhorst, D., Weisshaupt, A., Wedekind, F., Kroll, T., McCarley, R. W.,
520 Strecker, R. E., Bauer, A., 2015. Chronic sleep restriction induces long-lasting
521 changes in adenosine and noradrenaline receptor density in the rat brain. J Sleep
522 Res 24, 549-558.
523 Komori, T., Matsumoto, T., Motomura, E., Shiroyama, T., 2006. The sleep-enhancing
524 effect of valerian inhalation and sleep-shortening effect of lemon inhalation. Chem
525 Senses 31, 731-737.
526 Lambolez, B., Audinat, E., Bochet, P., Crepel, F., Rossier, J., 1992. AMPA receptor
527 subunits expressed by single Purkinje cells. Neuron 9, 247-258.

528 Lazarus, M., Chen, J. F., Urade, Y., Huang, Z. L., 2013. Role of the basal ganglia in the
529 control of sleep and wakefulness. Curr Opin Neurobiol 23, 780-785.
530 Lazarus, M., Shen, H. Y., Cherasse, Y., Qu, W. M., Huang, Z. L., Bass, C. E.,
531 Winsky-Sommerer, R., Semba, K., Fredholm, B. B., Boison, D., Hayaishi, O., Urade,
532 Y., Chen, J. F., 2011. Arousal effect of caffeine depends on adenosine A2A receptors
533 in the shell of the nucleus accumbens. J Neurosci 31, 10067-10075.
534 Murata, K., Kanno, M., Ieki, N., Mori, K., Yamaguchi, M., 2015. Mapping of Learned
535 Odor-Induced Motivated Behaviors in the Mouse Olfactory Tubercle. J Neurosci 35,
536 10581-10599.
537 Murphy, C., 1999. Loss of olfactory function in dementing disease. Physiol Behav 66,
538 177-182.
539 Oishi, Y., Suzuki, Y., Takahashi, K., Yonezawa, T., Kanda, T., Takata, Y., Cherasse, Y.,
540 Lazarus, M., 2017a. Activation of ventral tegmental area dopamine neurons produces
541 wakefulness through dopamine D2-like receptors in mice. Brain Struct Funct 222,
542 2907-2915.
543 Oishi, Y., Xu, Q., Wang, L., Zhang, B. J., Takahashi, K., Takata, Y., Luo, Y. J., Cherasse,
544 Y., Schiffmann, S. N., de Kerchove d'Exaerde, A., Urade, Y., Qu, W. M., Huang, Z. L.,
545 Lazarus, M., 2017b. Slow-wave sleep is controlled by a subset of nucleus
546 accumbens core neurons in mice. Nat Commun 8, 734.
547 Orr, A. G., Hsiao, E. C., Wang, M. M., Ho, K., Kim, D. H., Wang, X., Guo, W., Kang, J., Yu,
548 G. Q., Adame, A., Devidze, N., Dubal, D. B., Masliah, E., Conklin, B. R., Mucke, L.,

549 2015. Astrocytic adenosine receptor A2A and Gs-coupled signaling regulate memory.
550 Nat Neurosci 18, 423-434.
551 Qu, W. M., Xu, X. H., Yan, M. M., Wang, Y. Q., Urade, Y., Huang, Z. L., 2010. Essential
552 role of dopamine D2 receptor in the maintenance of wakefulness, but not in
553 homeostatic regulation of sleep, in mice. J Neurosci 30, 4382-4389.
554 Satoh, S., Matsumura, H., Koike, N., Tokunaga, Y., Maeda, T., Hayaishi, O., 1999.
555 Region-dependent difference in the sleep-promoting potency of an adenosine A2A
556 receptor agonist. Eur J Neurosci 11, 1587-1597.
557 Scott, J. W., McBride, R. L., Schneider, S. P., 1980. The organization of projections from
558 the olfactory bulb to the piriform cortex and olfactory tubercle in the rat. J Comp
559 Neurol 194, 519-534.
560 Sharma, R., Sahota, P., Thakkar, M. M., 2018. Severe and protracted sleep disruptions
561 in mouse model of post-traumatic stress disorder. Sleep 41.
562 Spiegelhalder, K., Regen, W., Nanovska, S., Baglioni, C., Riemann, D., 2013. Comorbid
563 sleep disorders in neuropsychiatric disorders across the life cycle. Curr Psychiatry
564 Rep 15, 364.
565 Venner, A., Anaclet, C., Broadhurst, R. Y., Saper, C. B., Fuller, P. M., 2016. A Novel
566 Population of Wake-Promoting GABAergic Neurons in the Ventral Lateral
567 Hypothalamus. Curr Biol 26, 2137-2143.
568 Wang, Y. Q., Li, R., Wang, D. R., Cherasse, Y., Zhang, Z., Zhang, M. Q., Lavielle, O.,
569 McEown, K., Schiffmann, S. N., de Kerchove d'Exaerde, A., Qu, W. M., Lazarus, M.,

570 Huang, Z. L., 2017. Adenosine A2A receptors in the olfactory bulb suppress rapid eye
571 movement sleep in rodents. Brain Struct Funct 222, 1351-1366.
572 Wang, Y. Q., Li, R., Wu, X., Zhu, F., Takata, Y., Zhang, Z., Zhang, M. Q., Li, S. Q., Qu, W.
573 M., 2015. Fasting activated histaminergic neurons and enhanced arousal effect of
574 caffeine in mice. Pharmacol Biochem Behav 133, 164-173.
575 Warre, R., Thiele, S., Talwar, S., Kamal, M., Johnston, T. H., Wang, S., Lam, D., Lo, C.,
576 Khademullah, C. S., Perera, G., Reyes, G., Sun, X. S., Brotchie, J. M., Nash, J. E.,
577 2011. Altered function of glutamatergic cortico-striatal synapses causes output
578 pathway abnormalities in a chronic model of parkinsonism. Neurobiol Dis 41,
579 591-604.
580 Wesson, D. W., Wilson, D. A., 2011. Sniffing out the contributions of the olfactory
581 tubercle to the sense of smell: hedonics, sensory integration, and more? Neurosci
582 Biobehav Rev 35, 655-668.
583 Xiong, A., Wesson, D. W., 2016. Illustrated Review of the Ventral Striatum's Olfactory
584 Tubercle. Chem Senses 41, 549-555.
585 Xu, M., Chung, S., Zhang, S., Zhong, P., Ma, C., Chang, W. C., Weissbourd, B., Sakai,
586 N., Luo, L., Nishino, S., Dan, Y., 2015. Basal forebrain circuit for sleep-wake control.
587 Nat Neurosci 18, 1641-1647.
588 Yamaoka, S., Tomita, T., Imaizumi, Y., Watanabe, K., Hatanaka, A., 2005. Effects of
589 plant-derived odors on sleep-wakefulness and circadian rhythmicity in rats. Chem
590 Senses 30 Suppl 1, i264-265.

591 Yuan, X. S., Wang, L., Dong, H., Qu, W. M., Yang, S. R., Cherasse, Y., Lazarus, M.,
592 Schiffmann, S. N., d'Exaerde, A. K., Li, R. X., Huang, Z. L., 2017. Striatal adenosine
593 A2A receptor neurons control active-period sleep via parvalbumin neurons in external
594 globus pallidus. Elife 6.
595 Zhang, J. P., Xu, Q., Yuan, X. S., Cherasse, Y., Schiffmann, S. N., de Kerchove
596 d'Exaerde, A., Qu, W. M., Urade, Y., Lazarus, M., Huang, Z. L., Li, R. X., 2013.
597 Projections of nucleus accumbens adenosine A2A receptor neurons in the mouse
598 brain and their implications in mediating sleep-wake regulation. Front Neuroanat 7,
599 43.
600 Zhang, M. Q., Wang, T. X., Li, R., Huang, Z. L., Han, W. J., Dai, X. C., Wang, Y. Q., 2017.
601 Helicid alleviates pain and sleep disturbances in a neuropathic pain-like model in
602 mice. J Sleep Res 26, 386-393.
603

Fig. 1. Activation of A_{2A}Rs in the OT increases NREM sleep in rats. (A and B) Typical examples of two rats injected with vehicle (A) or a selective A_{2A}R agonist CGS21680 at 0.6 nmol/side (B) into the OT. Freq: Frequency. (C and D) The hourly mean amount of NREM sleep, REM sleep and wakefulness during a 24-hour recording period are presented (C) along with the amounts of each stage during 21:00-02:00 and 02:00-07:00 (D). (E) NREM sleep power density curves during 21:00-02:00 after CGS21680 or vehicle injections are shown. (F) The position of the guide cannulae in the OT of one rat. The OT is highlighted by the pink area in the schematic 1.80 mm prior to bregma and a bright-field photomicrograph of a Nissl's stained coronal section illustrates the typical position of the guide cannulae. The white rectangle represents the guide cannulae which were inserted at an angle of 30 degrees against vertical, and the black rectangle represents the tip of the syringe. Scale bar =2 mm. Values are presented as means ± SEM (n =11). **p* <0.05, ***p* <0.01. Statistical analysis against the vehicle group was assessed by repeated ANOVA measurement (c) or by one-way ANOVA (d and e).

Fig. 2. Blockade of A_{2A}Rs in the OT decreases NREM sleep in rats. (A and B) Typical examples of two rats injected with vehicle (A) or a selective A_{2A}R antagonist KW6002 at 15.6 nmol/side (B) into the OT. Freq: Frequency. (C) NREM sleep latency after vehicle or KW6002 injection. (D) The hourly mean amount of NREM sleep, REM sleep, and wakefulness during a 24-hour recording period of vehicle- or KW6002- (15.6 nmol/side) injected rats (D) is shown. Values are means ± SEM (n=6-7). **p* <0.05, ***p* <0.01.

625 Statistical analysis against the vehicle group was assessed by repeated ANOVA
626 measurement (D) or one-way ANOVA (C).
627
628 **Fig. 3. Chemogenetic activation of OT A_{2A}R neurons via hM3Dq promotes NREM**
629 **sleep.** (A) A_{2A}R-Cre mice were infused with AAV expressing hM3Dq in a Cre-dependent
630 manner under the control of the A_{2A}R promotor (OT-hM3Dq mice). ITR: inverted terminal
631 repeat; hSyn: human synapsin promoter; WPRE: woodchuck hepatitis
632 posttranscriptional regulatory element. (B) Typical traces of an hM3Dq-expressing OT
633 A_{2A}R neuron bath applied with CNO at a concentration of 3 μM. (C) Firing frequency and
634 membrane potential elicited from CNO (3 μM) application to the electrophysiological bath.
635 (D) A heat map is shown the expression of hM3Dq-mCherry fusion protein in the OT of
636 A_{2A}R-Cre mice. The areas surrounded by the red dash line represent the OT. The color
637 bar indicates the level of mCherry expression across the OT of 10 mice. (E-H) Typical
638 samples of two OT-hM3Dq mice injected with either CNO (E and F) or vehicle (G and H).
639 The dashed line rectangle areas in e and g were magnified (F, H) to show the
640 co-expression of hM3Dq fusion protein and c-Fos, which is indicated by black arrows. (I
641 and J) Typical examples of one OT-hM3Dq mouse injected (i.p.) with vehicle (I) and CNO
642 at 3.0 mg/kg (J). Freq: Frequency. (K and L) The hourly mean amount of NREM sleep,
643 REM sleep, and wakefulness during a 24-hour recording period of vehicle- or
644 CNO-treated OT-hM3Dq mice (K) are shown along with the amounts of each stage
645 during 21:00-24:00 (L). Values are means ± SEM (n =10). (M) The hourly mean of NREM

646 sleep, REM sleep and wakefulness during a 24-hour recording period of vehicle- or
647 CNO-treated OT-hM4Di mice. Values are means ± SEM (n =9). *p <0.05, **p <0.01.
648 Statistical analysis against the vehicle treatment was assessed by two-tailed paired
649 Student's *t*-test in (C and L) and by repeated ANOVA measurement in (K and M).
650
651 **Fig. 4. The projection sites of OT A_{2A}R neurons in the brain.** (A) A schematic diagram
652 shows that A_{2A}R-Cre mice were injected with an AAV vector containing hrGFP, of which
653 the expression is controlled by the A_{2A}R promotor, into the OT. ITR: inverted terminal
654 repeat; Neo: neomycin-resistance gene. (B) A typical brain section expressing hrGFP in
655 the OT A_{2A}R neurons. The bottom right corner illustrates the morphology of
656 A_{2A}R-expressing neurons in the OT, which is magnified from the area in the white
657 rectangle. (C-H) The terminals of the OT A_{2A}R neurons were found in the external
658 plexiform layer (EPl) of the olfactory bulbs (C), secondary motor cortex (M2) (D), ventral
659 pallidum (VP) (E), piriform cortex (Pir), dorsal endopiriform nucleus (DEn) and ventral
660 endopiriform nucleus (VEn) (F), cortex-amygdala transition zone (CxA), dorsal part of
661 anterior amygdaloid area (AAD), anterior part of basomedial amygdaloid nucleus (BMA),
662 anterior cortical amygdaloid nucleus (ACo), nucleus of the lateral olfactory tract (LOT) (G)
663 and lateral hypothalamic area (LH) (H). A small schematic drawing of a coronal brain
664 section at the upper right corner in each panel indicates the location of the
665 photomicrograph in the mouse brain (red rectangular area). Scale bar =200 μm in (B);
666 scale bar =100 μm in (C-H).

667

668 **Fig. 5. Photostimulation of OT A_{2A}R neurons evokes GABA release in the VP and**
669 **LH.** (A) A schematic drawing shows ChR2-expressing OT and the targeted downstream
670 nuclei, the VP and the LH. (B) Electrophysiological properties of fluorescent
671 A_{2A}R-expressing neuron. (C) Different frequencies (5, 10 and 20 Hz) of photostimulation
672 (pulse width: 5 ms) were applied to the same recording neuron. (D) Single-cell RT-PCR
673 was utilized to separately determine the presence of vesicular GABA transporter (vGAT)
674 and vesicular glutamate transporter 2 (vGluT2) mRNA in the recorded OT A_{2A}R neurons.
675 (E and F) Typical traces (upper panel) representing the synchronized inward current
676 elicited by photostimulation of ChR2-expressing OT axons at VP under different
677 conditions and the according statistical data (lower panel). (G) The latency between the
678 delivery of photostimulation and the firing event of responding VP neurons (59.4%) are
679 summarized. (H) The presence of vGAT and vGluT2 mRNA was determined in the
680 responding VP neurons via single-cell RT-PCR. (I and J) Typical traces (upper panel)
681 representing the synchronized inward current elicited by photostimulation of
682 ChR2-expressing OT axons at LH under different conditions and the according statistical
683 data (lower panel). (K) The latency of responding LH neurons (24.2%) are summarized.
684 (L) Single-cell RT-PCR result of the responding LH neurons. Values are means ± SEM. n
685 =60 trials in (E, F, I and J). *p <0.05 and **p <0.01 denotes significantly different from the
686 base condition as assessed by paired t-test. #p <0.05 denotes significantly different

687 values from the glutamate receptor-blocking condition as assessed by two-tailed paired

688 Student's *t*-test.

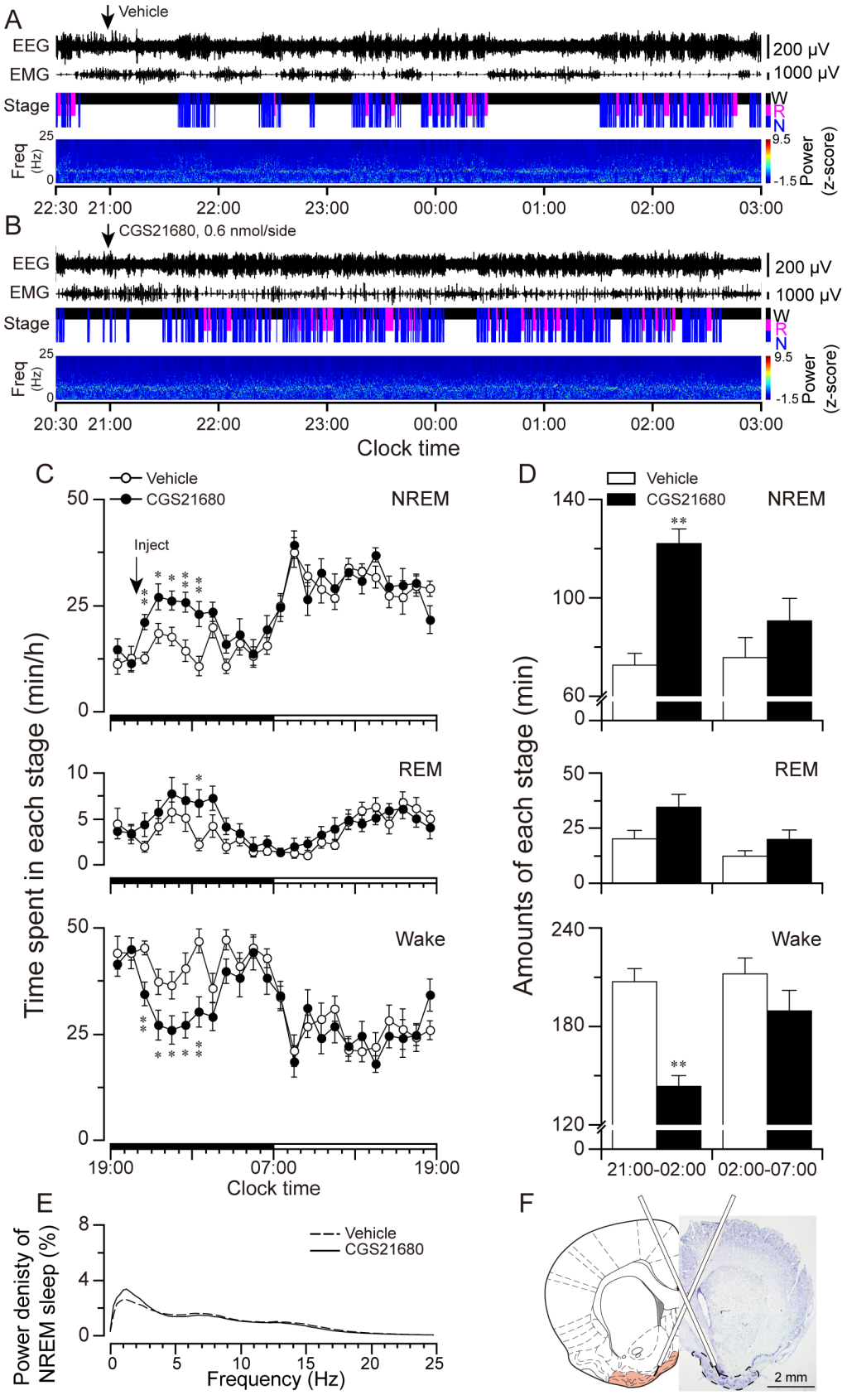
A
Vehicle
EEG
EMG
Stage
Freq (Hz)
200 μV
1000 μV
W
R
N
Power (z-score)
22:30 21:00 22:00 23:00 00:00 01:00 02:00 03:00
B
CGS21680, 0.6 nmol/side
20:30 21:00 22:00 23:00 00:00 01:00 02:00 03:00
Clock time
C
Vehicle
CGS21680
NREM
REM
Wake
Inject
Time spent in each stage (min/h)
19:00 07:00 19:00
Clock time
D
Amounts of each stage (min)
21:00-02:00 02:00-07:00
E
Power denisty of NREM sleep (%)
Frequency (Hz)
F
2 mm

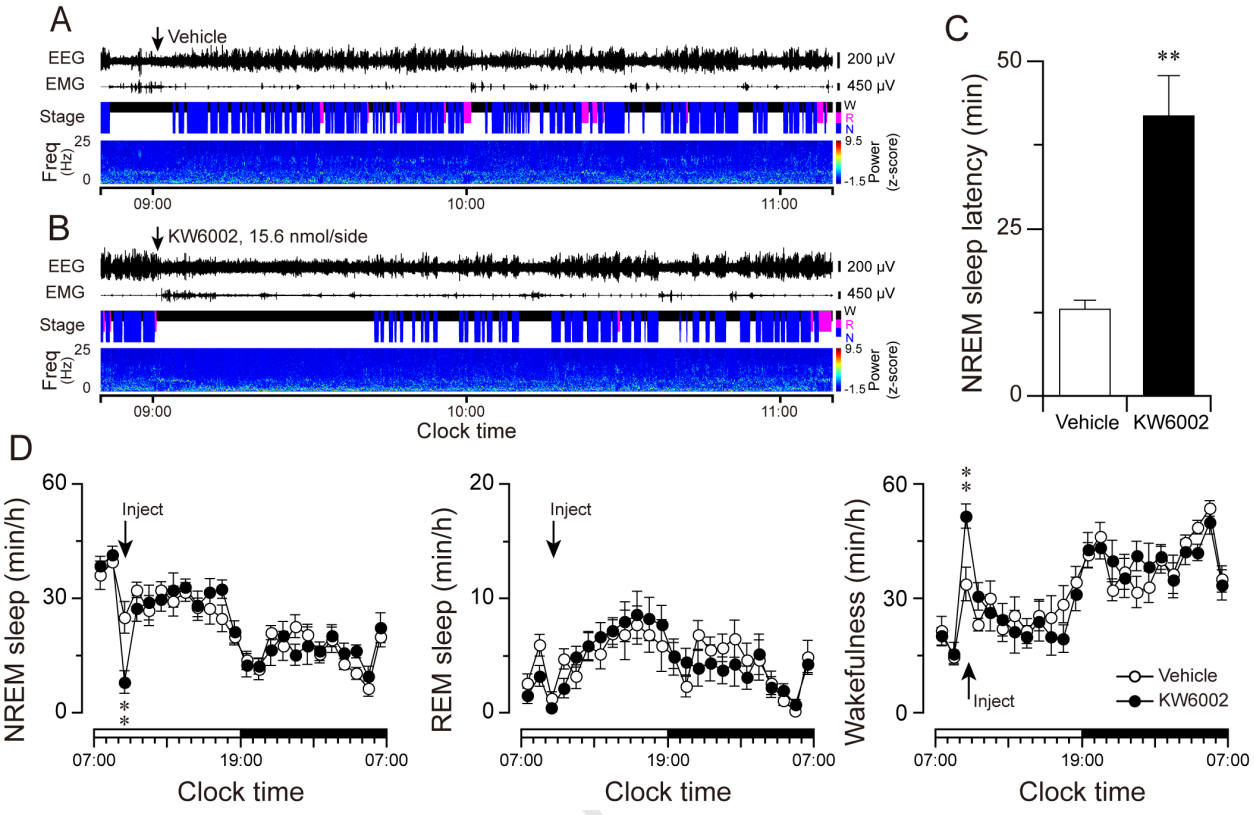

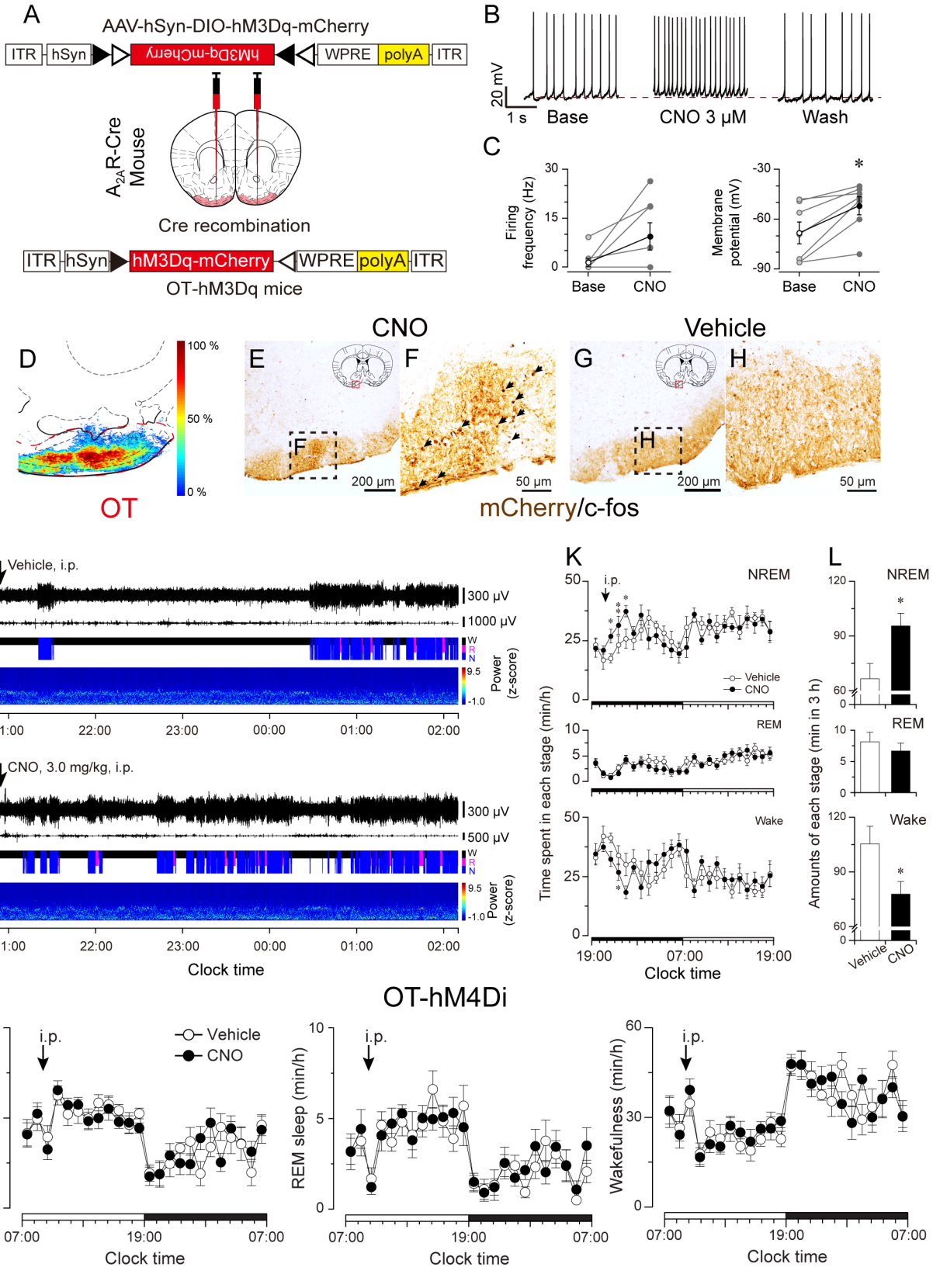
A
AAV-hSyn-DIO-hM3Dq-mCherry
ITR
hSyn
hM3Dq-mCherry
WPRE
polyA
ITR
A2AR-Cre Mouse
Cre recombination
ITR
hSyn
hM3Dq-mCherry
WPRE
polyA
ITR
OT-hM3Dq mice
B
20 mV
1 s
Base
CNO 3 μM
Wash
C
Firing frequency (Hz)
Base
CNO
Membrane potential (mV)
Base
CNO
CNO
Vehicle
D
100 %
50 %
0 %
OT
E
F
200 μm
50 μm
G
H
200 μm
50 μm
mCherry/c-fos
I
Vehicle, i.p.
EEG
EMG
Stage
Freq (Hz)
Power (z-score)
300 μV
1000 μV
21:00
22:00
23:00
00:00
01:00
02:00
J
CNO, 3.0 mg/kg, i.p.
EEG
EMG
Stage
300 μV
500 μV
Clock time
K
NREM
REM
Wake
i.p.
Vehicle
CNO
Time spent in each stage (min/h)
19:00
07:00
19:00
Clock time
L
NREM
REM
Wake
Amounts of each stage (min in 3 h)
Vehicle
CNO
M
OT-hM4Di
i.p.
Vehicle
CNO
NREM sleep (min/h)
REM sleep (min/h)
Wakefulness (min/h)
07:00
19:00
07:00
Clock time

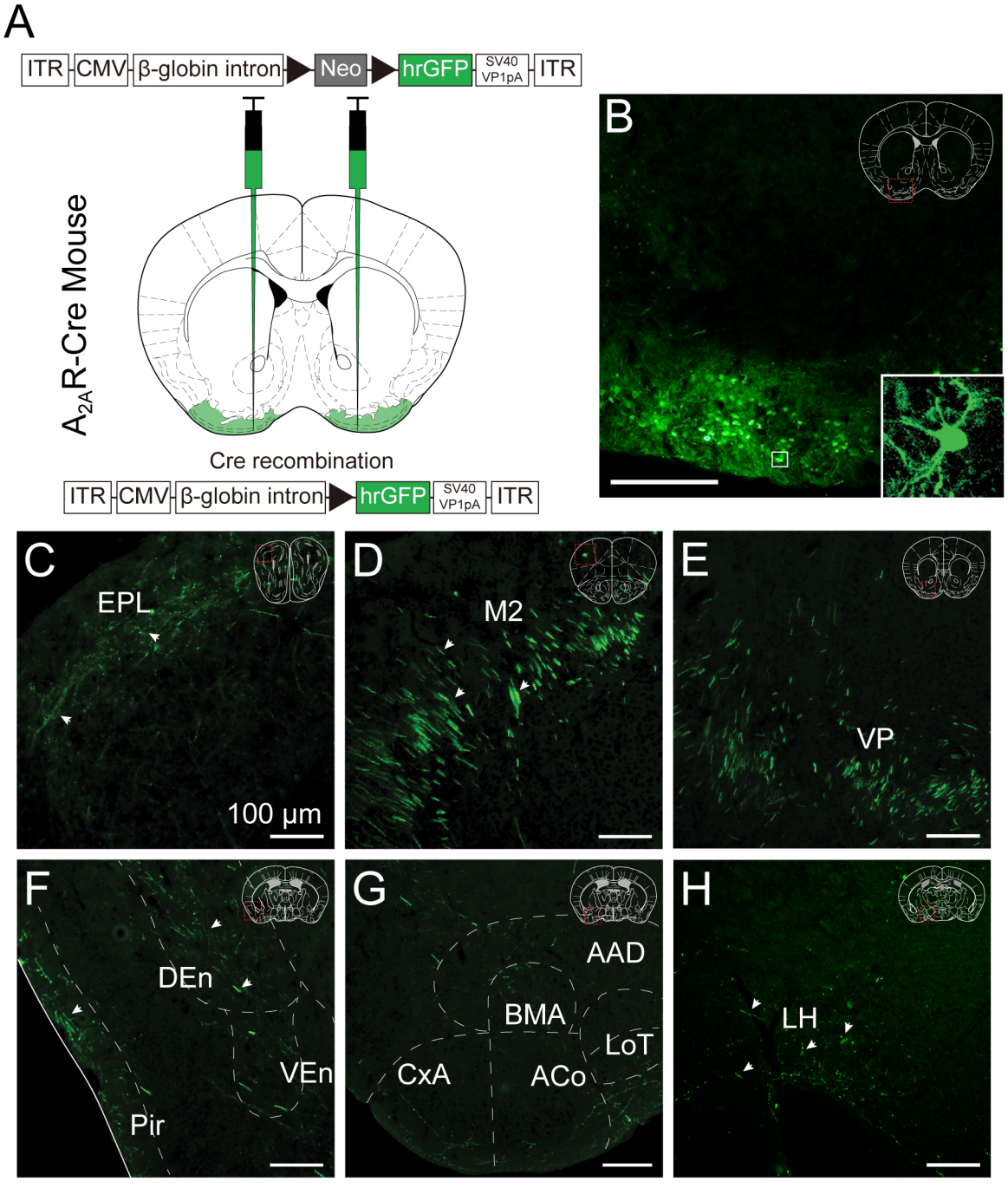
A
ITR
CMV
β-globin intron
Neo
hrGFP
SV40 VP1pA
ITR
A2AR-Cre Mouse
Cre recombination
ITR
CMV
β-globin intron
hrGFP
SV40 VP1pA
ITR
B
C
EPL
100 µm
D
M2
E
VP
F
DEn
VEn
Pir
G
AAD
BMA
LoT
CxA
ACo
H
LH

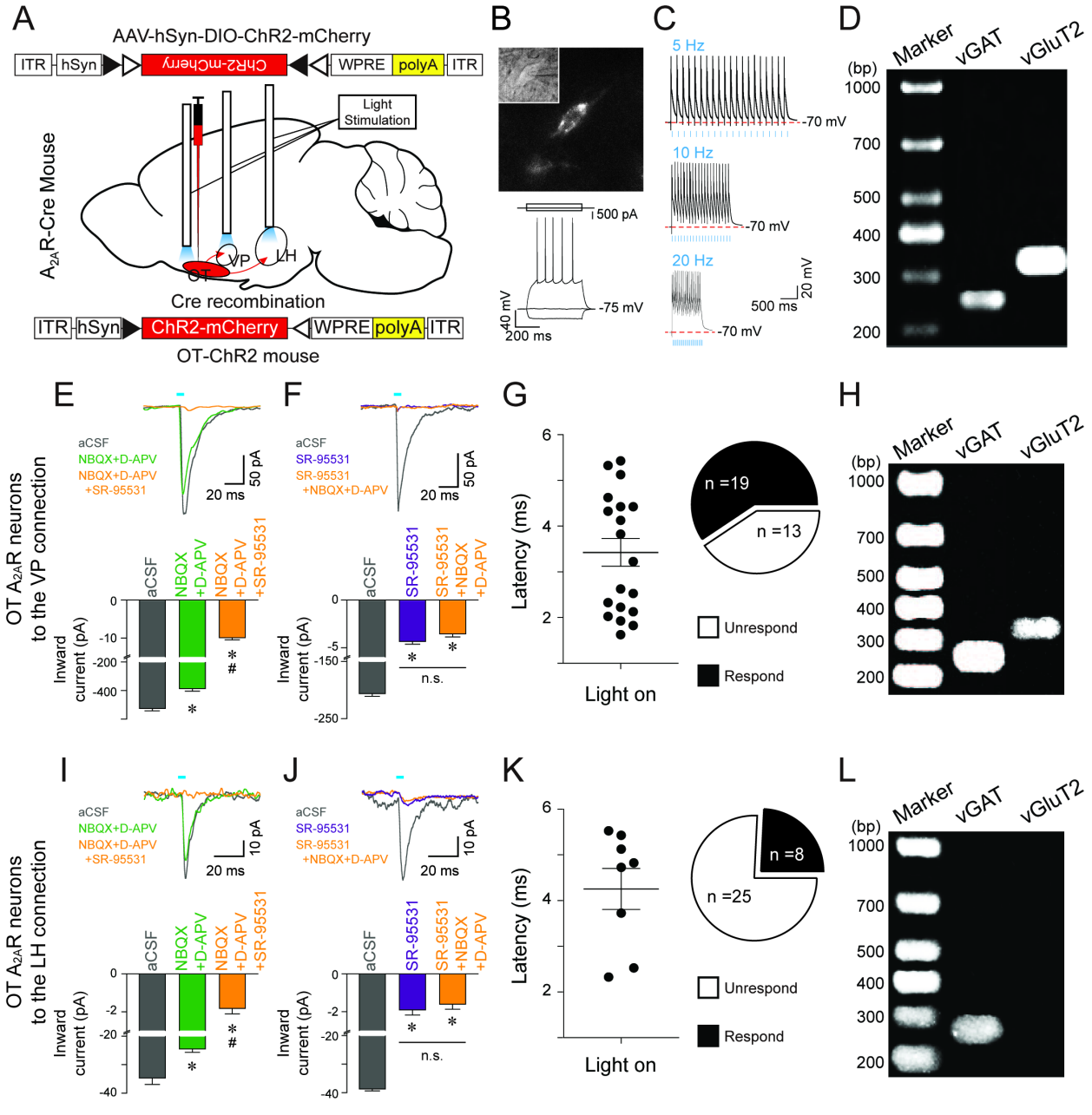
A
AAV-hSyn-DIO-ChR2-mCherry
ITR
hSyn
ChR2-mCherry
WPRE
polyA
ITR
Light Stimulation
A2AR-Cre Mouse
VP
LH
OT
Cre recombination
ITR
hSyn
ChR2-mCherry
WPRE
polyA
ITR
OT-ChR2 mouse
B
500 pA
40 mV
200 ms
-75 mV
C
5 Hz
-70 mV
10 Hz
-70 mV
20 Hz
-70 mV
500 ms
20 mV
D
Marker
vGAT
vGluT2
(bp)
1000
700
500
400
300
200
E
aCSF
NBQX+D-APV
NBQX+D-APV
+SR-95531
20 ms
50 pA
OT A2AR neurons
to the VP connection
aCSF
NBQX
+D-APV
NBQX
+D-APV
+SR-95531
Inward
current (pA)
0
-10
-200
-400
F
aCSF
SR-95531
SR-95531
+NBQX+D-APV
20 ms
50 pA
aCSF
SR-95531
SR-95531
+NBQX
+D-APV
Inward
current (pA)
0
-5
-150
-250
n.s.
G
Latency (ms)
6
4
2
Light on
n =19
n =13
Unrespond
Respond
H
Marker
vGAT
vGluT2
(bp)
1000
700
500
400
300
200
I
aCSF
NBQX+D-APV
NBQX+D-APV
+SR-95531
20 ms
10 pA
OT A2AR neurons
to the LH connection
aCSF
NBQX
+D-APV
NBQX
+D-APV
+SR-95531
Inward
current (pA)
0
-2
-20
-40
J
aCSF
SR-95531
SR-95531
+NBQX+D-APV
20 ms
10 pA
aCSF
SR-95531
SR-95531
+NBQX
+D-APV
Inward
current (pA)
0
-2
-20
-40
n.s.
K
Latency (ms)
6
4
2
Light on
n =8
n =25
Unrespond
Respond
L
Marker
vGAT
vGluT2
(bp)
1000
700
500
400
300
200

- Activation of OT A_{2A}Rs increased NREM sleep.
- Blockade of OT A_{2A}Rs increased sleep latency.
- Chemogenetic activation of OT A_{2A}R neurons increased NREM sleep.
- Connections between OT A_{2A}R neurons and neurons in the VP and LH were inhibitory.
- The study concluded that the OT promotes sleep through A_{2A}Rs and A2AR neurons.

The conception of the study, Y.Q.W. and Z.L.H; The design of the study, R.L., Y.Q.W., W.Y.L., and Z.L.H.; Acquisition of data, R.L., W.Y.L., M.Q.Z., and L.L.; Analysis and interpretation of data, R.L., Y.Q.W., and W.Y.L.; Resource: Y.C., S.N.S., A.K.E., and M.L.; Article drafting, R.L.; Article revising, R.L., Y.Q.W., W.Y.L., M.Q.Z., Y.C., M.L., Z.L.H..